Received: 26 April 2018 | Revised: 27 June 2018 | Accepted: 3 July 2018

DOI: 10.1002/aoc.4527

FULL PAPER

WILEY Applied Organometallic Chemistry

Synthesis, theoretical investigations, biocidal screening, DNA binding, *in vitro* cytotoxicity and molecular docking of novel Cu (II), Pd (II) and Ag (I) complexes of chlorobenzylidene Schiff base: Promising antibiotic and anticancer agents

Laila H. Abdel-Rahman[1] | Mohamed Shaker S. Adam[1,2] | Ahmed M. Abu-Dief[1] | H. Moustafa[3] | Maram T. Basha[4] | Ahmed S. Aboraia[5] | Badriah Saad Al-Farhan[6] | Hanan El-Sayed Ahmed[1]

[1] Chemistry Department, Faculty of Science, Sohag University, Sohag, Egypt

[2] Department of Chemistry, College of Science, King Faisal University, Al Hufuf, Al Hassa, Saudi Arabia

[3] Chemistry Department, Faculty of Science, Cairo University, Giza, Egypt

[4] Department of Chemistry, Faculty of Science, University of Jeddah, Jeddah, Saudi Arabia

[5] Medicinal Chemistry Department, Faculty of Pharmacy, Assiut University, Assiut, Egypt

[6] Department of Chemistry, Faculty of Girls for Science, King Khalid University, Abha, Saudi Arabia

Correspondence
Laila H. Abdel-Rahman and Ahmed M. Abu-Dief, Chemistry Department, Faculty of Science, Sohag University, Sohag 82534, Egypt.
Email: lailakenawy@hotmail.com, laila.abdelrahman@science.sohag.edu.eg; ahmed_benzoic@yahoo.com

Three new Cu (II), Pd (II) and Ag (I) complexes of bidentate Schiff base ligand 2-[(4-chlorobenzylidene)amino] phenol (HL) were synthesized. The stoichiometric ratios and physicochemical properties of these complexes were determined using elemental analyses, magnetic measurements, infrared and UV–visible spectra, molar conductivity measurements and thermal analyses. The results revealed that the metal ions coordinated with through azomethine nitrogen and phenolic oxygen atoms. AgL and PdL complexes are present in a 1:1 molar ratio with square planar and tetrahedral geometry, respectively, while CuL_2 complex is present in a 1:2 molar ratio with octahedral geometry. The electronic structure and nonlinear optical parameters of HL and the studied 1:1 and 1:2 complexes were investigated theoretically at the DFT-B3LYP/6-311G** level of theory. The compounds were screened against various strains of bacteria and fungi. They displayed good results for inhibition against the studied pathogenic microorganisms. Absorption spectroscopic, viscosity and gel electrophoresis measurements were used for studying the interaction of the prepared complexes with calf thymus DNA (CT-DNA). The studied complexes showed a good interaction with CT-DNA via intercalation and groove modes. Moreover, molecular docking of these complexes was studied to understand the drug–DNA interactions and calculate the potential binding mode and energy. The anticancer effects of HL and its complexes, on selected human carcinoma cell lines, were determined. The cytotoxicity results showed that the prepared complexes are more potent than the Schiff base ligand.

KEYWORDS
chlorobenzilidine, CT-DNA, cytotoxicity, docking, NLO properties

1 | INTRODUCTION

Schiff base ligands have received much attention in recent years due to their ability to coordinate with various metal ions and their potent applications in medicine and pharmacy because of their antibacterial,[1] anticancer,[2] antifungal,[3] anti-tubercular[4] and anti-inflammatory[5] activities. Bidentate Schiff base ligand of 2-aminophenol and 4-chlorobenzaldhyde has various clinical and biological applications.[6,7] In fact, Pd (II) complexes have a significant anti-tumour activity with minimum side effects compared to cisplatin which has some drawbacks such as nephrotoxicity, drug resistance and cervical renal problems.[8–10] Palladium (II) complexes show structural properties similar to those of Pt (II) and promising cytotoxicity, so they are suitable for metallodrugs. Silver (I) complexes have great biological therapeutic activities.[11] Furthermore, Cu (II) complexes are used as anticancer agents due to their selective permeability of cancer cell membranes. However, there is no systematic study of the electronic structures and nonlinear properties of the studied complexes. Therefore, such study is important for understanding the activity and nonlinear optical (NLO) properties of these complexes. Nonlinear optics explains the response of nonlinear properties such as polarization, frequency, path or phase of incident light.[12] One of the NLO phenomena is second harmonic generation where intense light of longer wavelength is converted to light of wavelength of half of the incident value, upon absorption by a NLO material.

From this point of view, the aim of the investigation reported here was to synthesize a Schiff base ligand from the condensation of 2-aminophenol and 4-chlorobenzaldehyde and its Pd (II), Ag (I) and Cu (II) complexes and to characterize them via various analytical and physical tools. The geometrical parameters, electrostatic potential and natural bond order (NBO; natural charges, natural population and natural configuration) of the investigated ligand and its complexes were calculated, using B3LYP/6-311G**. The electronic dipole moment (μ) and first-order hyperpolarizability (β) values of the studied complexes were computed to study the NLO properties. Global reactivity descriptors, namely electronegativity (χ), hardness (η) and softness (S), of the studied complexes were calculated and analysed. Moreover, antibacterial and antifungal bioassays were conducted and the interaction with calf thymus DNA (CT-DNA) of these complexes was evaluated. In addition to that, we investigated their anticancer activity towards various cancer cell lines. Biological applications of the prepared compounds were confirmed via performing molecular docking study.

2 | EXPERIMENTAL

The materials and instrumentation used in this study are given in the supporting information (S1).

2.1 | Synthesis of Ligand

The ligand 2-[(4-chlorobenzylidene)amino] phenol (HL) was synthesized by adding an ethanolic solution (20 ml) of 4-chlorobenzaldehyde (10 mmol, 1.40 g) to an ethanolic solution (20 ml) of 2-aminophenol (10 mmol, 1.09 g). This mixture was stirred under reflux at 70°C for 2 h using triethylamine as a catalyst and then allowed to cool to room temperature to afford a yellow solid precipitate. The obtained precipitate was then filtered and washed with ethanol.

Yield 78%; yellow colour; m.p. >115°C. FT-IR (KBr, cm^{-1}): 1624 (C=N), 3302 (—OH). ^{1}H NMR (DMSO-d_6, δ, ppm): 8.98 (s, 1H, OH), 8.73 (s, 1H, N=CH), 7.24–7.22 (d, 2H, $2CH_{ar}$), 7.10–7.08 (d, 2H, $2CH_{ar}$), 6.92–6.90 (d, 2H, $2CH_{ar}$), 6.85–6.83 (d, 2H, $2CH_{ar}$). ^{13}C NMR (DMSO-d_6, δ, ppm): 114.83 (CH), 115.16 (CH), 116.42 (CH), 117.32 (CH), 119.58 (CH), 120.14 (CH), 128.19 (CH), 129.25 (CH), 129.8 (CH), 130.88 (C_q, CH—Cl), 131.64 (C_q, CH—CH=N), 158.50 (C_q, CH—OH), 192.75 (CH=N). Anal. Calcd for $C_{13}H_{10}NClO$ (%): C, 67.39; H, 4.32; N, 6.05. Found (%): C, 67.30; H, 3.8; N, 6.13.

2.2 | Synthesis of Metal Complexes

2.2.1 | Synthesis of CuL_2 complex

$CuCl_2{\cdot}2H_2O$ (5 mmol, 0.85 g) was dissolved in 20 ml of commercial ethanol and added to HL (10 mmol, 2.31 g) dissolved in acetone (20 ml). Then, the obtained mixture was stirred for 1 h and evaporated overnight to afford a black complex precipitate. The obtained precipitate was filtered, washed with ethanol and finally kept in a desiccator.

2.2.2 | Synthesis of PdL complex

The PdL complex was synthesized by mixing 5 mmol of Pd $(OAc)_2$ (1.12 g) dissolved in acetone (20 ml) with 5 mmol of HL (1.15 g) dissolved in acetone (20 ml). The solution was stirred under reflux at 50°C for 2 h to afford a dark brown precipitate. Then, the obtained precipitate was filtered, washed with ethanol and dried over anhydrous $CaCl_2$.

^{1}H NMR (DMSO-d_6, δ, ppm): 8.29 (s, 1H, N=CH), 7.43–7.42 (d, 2H, $2CH_{ar}$), 7.26–7.21 (d, 2H, $2CH_{ar}$), 7.08–7.06 (d, 2H, $2CH_{ar}$), 6.36–6.32 (d, 2H, $2CH_{ar}$), 2.49 (s, 3H, $OCOCH_3$).

2.2.3 | Synthesis of AgL complex

The AgL complex was prepared by mixing $AgNO_3$ (5 mmol, 0.849 g) dissolved in commercial ethanol (20 ml) with HL (5 mmol, 1.15 g) dissolved in acetone (20 ml) and was stirred for 1 h, whereupon a black complex precipitated. This precipitate was collected by filtration, purified by washing several times with diethyl ether and dried over anhydrous $CaCl_2$.

^{1}H NMR (DMSO-d_6, δ, ppm): 8.23 (s, 1H, N=CH), 7.48–7.45 (d, 2H, $2CH_{ar}$), 7.27–7.25 (d, 2H, $2CH_{ar}$), 7.19–7.08 (d, 2H, $2CH_{ar}$), 6.80–6.47 (d, 2H, $2CH_{ar}$).

2.3 | Estimation of Stoichiometry of Complexes

Estimation of stoichiometry for the prepared complexes was done from the molar ratio and the continuous variation methods.[13–15] Metal salt and ligand solutions were combined, stirred and allowed to equilibrate. The absorbance was measured at λ_{max} for each solution and plotted against the mole fraction of metal ion or the mole fraction of ligand.

2.4 | Estimation of Apparent Formation Constants of Complexes

From the results of the continuous variation method, the PdL and AgL complexes are present in a 1:1 molar ratio while the CuL_2 complex is present in a 1:2 molar ratio. Thus the formation constants (K_f) of these complexes were obtained from spectrophotometry measurements according to the following relations[16,17]:

$$K_f = \frac{A/A_m}{(1-A/A_m)^2 C} \quad \text{in the case of 1:1 molar ration} \tag{1}$$

$$K_f = \frac{A/A_m}{4(1-A/A_m)^3 C^2} \quad \text{in the case of 1:2 molar ration} \tag{2}$$

where A is arbitrarily selected from the values of absorbance on either side of the absorbance peak, A_m is maximum absorbance for the prepared complexes and C is the primary molar metal concentration. Also, $\Delta G^{\neq}$(the free energy change of the complexes) was determined at 25°C using the following relation[16,17]:

$$\Delta G^{\neq} = -RT \ln K_f \tag{3}$$

where K_f is the formation constant, R is the gas constant and T is the temperature in kelvin.

2.5 | Kinetic Studies of Schiff Base Metal Complexes

The integral method of the Coats–Redfern equation was used for determining the kinetic parameters of the decompositions process for the metal complexes according to the following equation[17,18]:

$$\log\left[\frac{\log[w_\infty/(w_\infty - w)]}{T^2}\right] = \log\left[\frac{AR}{\phi E^*}\left(1-\frac{2RT}{E^{\neq}}\right)\right] - \frac{E^{\neq}}{2.303RT} \tag{4}$$

where w_∞ is the mass loss at the accomplishment of the decomposition reaction, w is the mass loss at temperature T, $\phi$is the rate of heating and R is the universal gas constant. The left-hand side of equation (4) is plotted against $1/T$ since $1 - 2RT/E^* \approx 1$. $E^{\neq}$and A were estimated from the slope and the intercept of this plot, respectively. The enthalpy of activation ($\Delta H^{\neq}$), the entropy of activation ($\Delta S^{\neq}$) and the activation free energy change ($\Delta G^{\neq}$) were determined from the following relations[16–18]:

$$\Delta H^{\neq} = E^{\neq} - RT \tag{5}$$

$$\Delta S^{\neq} = 2.303R \log\left(\frac{Ah}{k_b T}\right) \tag{6}$$

$$\Delta G^{\neq} = \Delta H^{\neq} - T\Delta S \tag{7}$$

where h and k_b are the Planck and Boltzmann constants, respectively.

2.6 | Computational Methods

All computations were carried out using the Gaussian 09W software package.[19] Molecular geometries of all the studied complexes were fully optimized using the B3LYP/GENECP level of theory. For H, C, N, Cl and O atoms, the 6-311G** basis set was used and Los Alamos National Laboratory Double Zeta (LANL2DZ) basis set for Ag, Cu and Pd atoms.[20–23] During the geometry optimization, no symmetry constraints were applied.[24] HOMO and LUMO energy values of complexes were utilized to calculate the electronegativity and chemical hardness as follows: $\chi = (I + A)/2$ (electronegativity), $\eta = (I - A)/2$ (chemical hardness), $S = 1/2\eta$(chemical softness), where I and A are ionization potential and electron affinity, respectively, and $I = -E_{HOMO}$ and $A = -E_{LUMO}$.[25,26] NBO calculations were carried out at the B3LYP/6-31G** level to qualitatively calculate the intermolecular charge delocalization in the complexes. Throughout this work, molecular orbitals were constructed using the GaussView

5.08 visualization program.[27] The total static dipole moment (μ), the mean polarizability $<\alpha>$, the anisotropy of the polarizability $\Delta\alpha$and the mean first hyperpolarizability $<\beta>$ using the x, y, z components were calculated using the following equations[28,29]:

$$u = \left(u_x^2 + u_y^2 + u_z^2\right)^{1/2} \quad (8)$$

$$\alpha = \frac{\left(\alpha_{xx} + \alpha_{yy} + \alpha_{zz}\right)}{3} \quad (9)$$

$$\Delta\alpha = \left(\left(\alpha_{xx} - \alpha_{yy}\right)^2 + \left(\alpha_{yy} - \alpha_{zz}\right)^2 + \left(\alpha_{zz} - \alpha_{xx}\right)^2\right)^{1/2} \quad (10)$$

$$\beta = \left(\beta_x^2 + \beta_y^2 + \beta_z^2\right)^{1/2} \quad (11)$$

$$\beta_x = \beta_{xxx} + \beta_{xyy} + \beta_{xzz} \quad (12)$$

$$\beta_y = \beta_{yyy} + \beta_{xxy} + \beta_{yzz} \quad (13)$$

$$\beta_z = \beta_{zzz} + \beta_{xxz} + \beta_{yyz} \quad (14)$$

2.7 | Antibacterial Bioassay

The antibacterial activities of the synthesized compounds were screened against three bacterial strains, *Escherichia coli* (−ve), *Bacillus subtilis* (+ve) and *Staphylococcus aureus* (+ve), using the agar well dilution method.[30–35] The compounds were dissolved in dimethylsulfoxide (DMSO) with concentrations of 10 and 20 mg ml^{-1}. Nutrient agar was prepared, then sterilized in an autoclave and poured in sterile Petri plates. After cooling of nutrient agar in the Petri plates, the studied organisms were grown on the agar. After that, sterile paper discs (Whatman) each saturated with a solution of the prepared compounds were placed in the agar by working holes using a sterile cork borer. The Petri dishes were incubated for 24 h at 37°C.[30–36] The standard drug gentamycin was screened under similar conditions for comparison. DMSO has no activity against the microbial strains and was used as a negative control.

2.8 | Antifungal Bioassay

The antifungal activities of the synthesized ligand and its complexes were studied against three fungal strains, *Candida albicans*, *Aspergillus flavus* and *Trichophyton rubrum*, using the well diffusion method with potato dextrose agar as the environment.[30–36] These fungal species were separated from the infected parts of the host plant. The fungal strains were directly mixed with potato dextrose agar and dispersed into Petri dishes. Filter paper discs were saturated with DMSO solutions of the studied compounds with concentrations of 10 and 20 mg ml^{-1}. These plates were placed in an incubator at 35°C for 72 h. The results were recorded as zones of inhibition and were compared with fluconazole as standard drug.

2.9 | Binding of Schiff Base Metal Complexes with CT-DNA

CT-DNA was dissolved in Tris–HCl buffer (60 mM, pH = 7.2) by sonication. CT-DNA was sufficiently free from protein contamination such that CT-DNA solution gave a ratio of UV absorption at 260/280 nm equal to 1.92. The stock solution of CT-DNA was stored at 4°C.

2.9.1 | Electronic spectroscopy for interaction of complexes with CT-DNA

The complexes were dissolved in dimethylformamide (DMF) solvent. Electronic spectra were obtained by keeping the complex concentrations constant while changing the CT-DNA concentration in the interaction medium. The absorption due to free CT-DNA was eliminated by adding an appropriate amount of CT-DNA to both complex solution and reference solution and the spectral data obtained were considered to result from the DNA–metal complex aggregation. From the electronic spectral data, K_b (the intrinsic binding constant) was estimated from plotting $[DNA]/(\varepsilon_a - \varepsilon_b)$ versus [DNA] according to the following relation[30–35]:

$$\frac{[DNA]}{\varepsilon_a - \varepsilon_f} = [DNA]\frac{1}{\varepsilon_b - \varepsilon_f} + \frac{1}{K_b}\frac{1}{\varepsilon_b - \varepsilon_f} \quad (15)$$

where [DNA] is the molar concentration of CT-DNA in base pairs, ε_f, ε_a and ε_b are the extinction coefficients of free, apparent and fully bound complex, respectively. Parameters ε_f and ε_a were estimated from the isolated metal complex calibration curve A_{abs}/[complex] and DNA calibration curve A_{abs}/[DNA], respectively. K_b was calculated from the ratio of slope to intercept of this plot. $\Delta G_b^{\neq}$(standard Gibbs free energy) for DNA binding was calculated from the following equation[30–35]:

$$\Delta G_b^{\neq} = -RT \ln K_b \quad (16)$$

2.9.2 | Viscosity measurements for interaction of complexes with CT-DNA

An Oswald micro-viscometer was used for measuring the viscosity of the synthesized complexes with CT-DNA at a

constant temperature of 25°C. With maintaining the concentration of CT-DNA constant (420 μM), the fluidity times were registered for various concentrations of the complexes (0–250 μM). Bubbling nitrogen gas was used to mix the solution through the viscometer. The viscosity of the complexes with CT-DNA was measured from the mean value of three readings. The relative viscosity for the complexes with CT-DNA ($\eta°$) was estimated from the following relation[30–35]:

$$\eta = \frac{t - t^{\circ}}{t^{\circ}} \tag{17}$$

where t is the time for fluidity observed in seconds, $t°$ is the time for fluidity of buffer in seconds and $\eta/\eta°$ (the relative viscosity) was plotted against $1/R$, where

$$R = \frac{[\text{DNA}]}{[\text{complex}]} \tag{18}$$

2.9.3 | Gel electrophoresis for interaction of complexes with CT-DNA

Gel electrophoresis is used as a method for studying the binding of complexes with DNA.[30–35,37] The complexes were added to CT-DNA in equal volume and incubated at 37°C for 1 h. After that, the mixtures were mixed with DNA Loading Dye at a 1:1 molar ratio and then loaded onto the gel (1%) in TAE buffer. A constant voltage (100 V) was applied for 60 min. Finally, the gel was imagined under UV light using a transilluminator. Panasonic DMC-LZ5 Lumix DNA gel documentation system (In genius3) was used for photographing the illuminated gel.

2.10 | Molecular Docking

A Dell Precision™T3600 Workstation (Intel Xeon E5-1660 3.3 GHz, ECC RDIMM 1 TB (7200 RPM), 1 GB NVIDIA Quadro 2000, 16 GB 1600 MHz DDR3, Windows 7 Professional (64 bit)) was used to study the molecular docking of the complexes. Molecular Operating Environment MOE package version 2016.08 was used for the docking studies. X-ray crystal structure of a B-DNA dodecameric d (CGCG AATTCGCG)$_2$ running 3′-5′direction (PDB ID: 1BNA) was used to study the docking at 1.9 Å resolution. The structure of DNA was imported into MOE and hydrogen atoms were added and then subjected to the optimization of energy. The resulting model was subjected the search of systematic conformation with a gradient of RMS of 0.01 kcal mol^{-1} using default parameters in the Site Finder tool embedded in MOE. HL and its complexes were visualized by ChemBioDraw Ultra 12.0 for further preparation in the MOE. HL and its complexes were prepared for molecular docking through the following steps: hydrogen atoms were added, conformational search was applied to all the compounds and the best conformers underwent energy decrease using the MMFF94 force field.[38] Energy decrease with the steepest algorithm was applied, after which conjugate gradient method was run until it reached an RMS gradient of 0.00001 kcal mol^{-1} Å^{-1}. A database of HL and its complexes was generated for further docking studies. The standard protocol of the docking was used in MOE 2016.08. The Alpha Triangle placement that derives poses by random superposition of the ligand HL atom triplets alpha sphere dummies in the target site was used to detect the poses. The London dG scoring function estimated the free binding energy of the ligand from a given pose. A number of 50 cycles of calculation was used to estimate the best poses of the docked molecules. The produced dock file was created with different poses for the investigated ligand and arranged according to the final score function (S). S is the score of the last stage that was not set to None. The database browser was used for examining the different poses that were selected for the best ones.

2.11 | Anticancer Activity

The studied compounds were examined against Hep-G2 cell line (hepatocellular carcinoma), MCF-7 cell line (breast carcinoma) and HCT-116 cell line (colon carcinoma) at Cairo University, Pharmacology Department, Cancer Biology Department and the National Cancer Institute. The absorbance for each well was determined with an ELISA microplate reader (Σ960, Meter Tech, USA) at 564 nm. Firstly, in a 96-multiwell plate, cells were placed (104 cells per well) for 24 h at 37°C. Secondly, various concentrations in DMSO of the compounds (0, 1, 2.5, 5 and 10 μM) were added to this plate. Thirdly, the plate was incubated for 48 h at 37°C and in an atmosphere of 5% CO_2. After that, the plate was fixed, rinsed and stained with sulforhodamine B stain. Acetic acid was used to remove excess stain and then the plate was treated with Tris–EDTA buffer. An ELISA reader was used to measure the intensity of colour. The inhibitory concentration (IC_{50}) was estimated according to the following equation[30–32,37]:

$$IC_{50}\ (\%) = \frac{\text{Control}_{OD} - \text{compound}_{OD}}{\text{Control}_{OD}} \times 100 \tag{19}$$

3 | RESULTS AND DISCUSSION

3.1 | Infrared (IR) Spectroscopy

The nature of functional groups bonded to the metal ions was identified using IR spectroscopy. The IR characteristic

frequencies for HL and its complexes along with their assignments (Figures S1 and S2) are recorded in Table 1. Bands due to —OH and —CH=N groups are distinctive and offer proof regarding the structure of HL and its bonding with metals. A band at 1624 cm^{-1} in the ligand spectrum is due to —C=N bond stretching vibration. On complexation, this band is shifted to 1586, 1590 and 1630 cm^{-1} in the spectra of CuL_2, PdL and AgL, respectively. The change of this band is a distinct indication of the involvement of the azomethine nitrogen atoms in complex formation.[30,39] This is supported by the appearance of bands at 543, 501 and 515 cm^{-1} corresponding to the stretching vibration of M—O bond for CuL_2, PdL and AgL, respectively. Bands at 483, 435 and 475 cm^{-1} correspond to the stretching vibration of M—N bond in CuL_2, PdL and AgL, respectively.[33–35] The band at 3302 cm^{-1} observed in the ligand spectrum is due to stretching vibrations of free —OH. This band is shifted to 3316, 3424 and 3424 cm^{-1} in the spectra of CuL_2, PdL and AgL, respectively. The band at 828–834 cm^{-1} (OH rocking) suggests the presence of coordinated water in all the prepared complexes.[40] In the low-frequency region, th ligand spectrum shows an absorption band at 1198 cm^{-1} which can result from the stretching vibration for the phenolic group (CO). The shifting of that band to lower wavenumber on coordination shows that the oxygen atoms of the phenolic groups are coordinated to the metal centre.[30]

3.2 | ^{1}H NMR and ^{13}C NMR Spectra

NMR spectroscopy was used to confirm the identity of the compounds. The ^{1}H NMR spectrum of HL (Figure S3) shows two singlet signals at 8.73 and 8.98 ppm assigned to azomethine (CH=N) proton and one phenolic —OH. Moreover, it shows multiple signals at 6.83–7.24 ppm for eight aromatic protons. The higher values of δ for the —OH group can be assigned to the presence of intermolecular hydrogen bonding.[41] For the PdL and AgL complexes (Fig. S4), their ^{1}H NMR spectra show singlet signals at 8.23 and 8.29 ppm which are assigned to azomethine (CH=N) proton, respectively, so the change of the position of HC=N group signal indicates that it participates in bonding with the metal ions. The hydroxyl group signal disappeared on complexation with metal ions indicating its involvement in coordination.[42] The ^{1}H NMR spectrum of the PdL complex shows a singlet signal at 2.45 ppm which is assigned to ($OCOCH_3$) protons, indicating that this group binds to the metal ions in the complex. The ^{1}H NMR spectrum of CuL_2 cannot be measured due to the interference of its paramagnetic properties.[30]

The ^{13}C NMR spectrum of HL (Figure S5) exhibits a signal at 192.75 ppm that may be assigned to azomethine carbon. The signals appearing in the region 114.83–158.50 ppm are assigned to phenyl carbons.

3.3 | Electronic Spectroscopy

The electronic spectral data coupled with magnetic moment values suggest a structural geometry for the prepared complexes.[43] Electronic spectroscopy was used for confirming the stereochemistry of metal ions in the complexes depending on the positions and number of d–d transition peaks.[30–32,37] The values of the maximum absorption wavelength (λ_{max}) and the molar absorptivity (ε_{max}) are listed in Table 2 and the spectra are presented in Figure 1. The electronic absorption spectra of HL and its complexes were recorded in the wavelength range 200–800 nm and at 298 K. The n → π^* transition of HL appeared around λ_{max} = 288 nm in the UV–visible region. The ligand-to-metal charge transfer (LMCT) band appears around λ_{max} = 483, 489 and 468 nm in the absorption spectra of CuL_2, PdL and AgL, respectively. The d → d transition band for the CuL_2, PdL and AgL complexes appears in the region 501–557 nm.

3.4 | Spectrophotometric Determination of Stoichiometry of Complexes

3.4.1 | Continuous variation and molar ratio methods

Continuous variation and molar ratio methods were used for determining the stoichiometry of the prepared complexes.[44–48] The continuous variation curve displays absorbance maximum at a mole fraction of ligand of 0.5–0.7 showing the complexation of Cu (II) ion to the ligand in a molar ratio of 1:2 and of Pd (II) and Ag (I) ions

TABLE 1 Characteristic IR bands (cm^{-1}) of HL and its metal complexes

Compound	ν(OH)/H_2O	$\nu(CH)_{ar}$	ν(C=N)	ν(C—O)	ν(M—O)	ν(M—N)
HL	3302	3044	1624	1198	—	—
CuL_2	3316	3051	1586	1087	543	483
PdL	3424	3054	1590	1150	501	435
AgL	3423	3071	1630	1114	515	475

TABLE 2 Electronic spectral measurements of HL and its metal complexes

Compound	λ_{max} (nm)	ε (dm^3 mol^{-1} mm^{-1})	Assignment
HL	239	536.87	π→π*
	251	539.82	π→π*
	288	539.82	n→π*
	354	395.28	Intra-ligand band
CuL_2	239	5375.37	π→π*
	251	5795.80	π→π*
	288	5915.91	n→π*
	360	5135.13	Intra-ligand band
	483	5675.68	LMCT band
	557	3423.42	d–d band
PdL	239	5075.08	π→π*
	251	5195.20	π→π*
	288	5375.37	n→π*
	355	4504.50	Intra-ligand band
	489	5075.38	LMCT band
	525	5165.17	d–d band
AgL	239	1990.00	π→π*
	246	1960.00	π→π*
	409	465.00	Intra-ligand band
	468	370.00	LMCT band
	501	340.00	d–d band

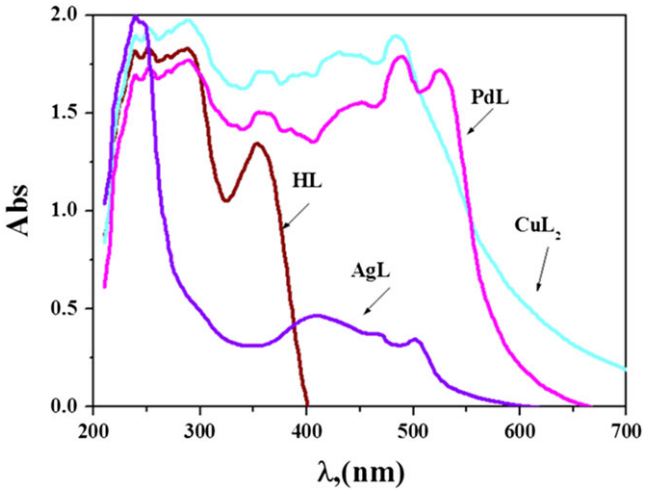

FIGURE 1 Electronic spectra of HL and its metal complexes in DMF at 298 K

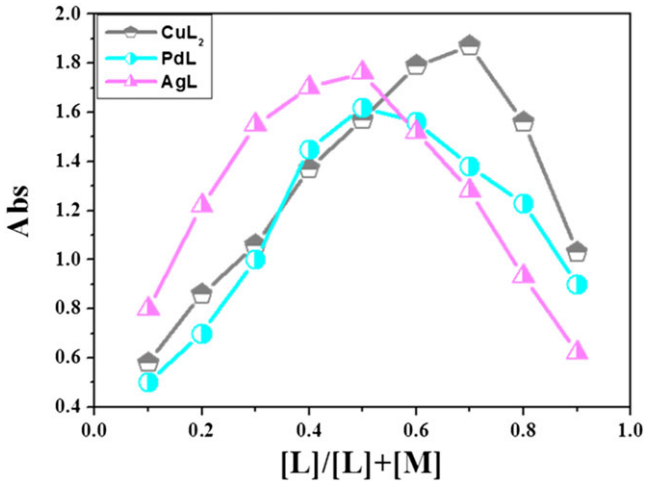

FIGURE 2 Curves of Job's method of the metal complexes in aqueous ethanol medium at [HL] = [M] = 10^{-3} M at 298 K

to the ligand in a molar ratio of 1:1 (Figure 2). The molar ratio curve confirmed the same molar ratio of metal ions to ligand (Figure S6).

3.4.2 | Determination of apparent formation constants for complexes

The formation constants (K_f) of the prepared complexes were calculated from spectrophotometry measurements by utilizing the continuous variation method (Table 3). The obtained K_f values show the high stability of the prepared complexes. The K_f values increase in the following order: AgL <PdL <CuL_2. Moreover, the stability constant (pK) and Gibbs free energy ($\Delta G^{\neq}$) values of the complexes were estimated. The negative values of Gibbs free energy show that the reaction is spontaneous and favoured.[13–17]

3.5 | Elemental Analyses

The elemental analyses results for HL and its complexes are listed in Table 4. These suggest that HL forms complexes

TABLE 3 Values of formation constant (K_f), stability constant (pK) and Gibbs free energy ($\Delta G^{\neq}$) for Schiff base metal complexes

Complex	Type of complex	K_f	pK	$\Delta G^{\neq}$(kJ mol^{-1})
CuL_2	1:2	10.88×10^9	10.04	−57.26
PdL	1:1	14.38×10^5	6.16	−35.13
AgL	1:1	1.90×10^5	5.28	−30.11

TABLE 4 Physical and analytical data of HL and its metal complexes

Compound Molecular formula	Molecular weight	Colour	M.p. and dec. temp. (°C)	Λ_m (Ω^{-1} cm^2 mol^{-1})	μ_{eff} (BM)	Analysis: found (calcd) C (%)	H (%)	N (%)
HL $C_{13}H_{10}NClO$	231.5	Yellow	115	—	—	67.30 (67.39)	4.38 (4.32)	6.13 (6.05)
CuL_2 $C_{26}H_{24}N_2Cl_2O_5Cu$	578.5	Black	(<300)	20.80	1.47	54.03 (53.93)	4.07 (4.15)	4.90 (4.84)
PdL $C_{15}H_{14}NClO_4Pd$	413.9	Dark brown	(<300)	4.00	Diamagnetic	43.59 (43.49)	3.50 (3.38)	3.46 (3.38)
AgL $C_{13}H_{13}NClO_3Ag$	374.3	Black	(<300)	7.70	Diamagnetic	41.80 (41.68)	3.40 (3.47)	3.86 (3.74)

with Cu (II) ion in a molar ratio of 1:2 and with Pd (II) and Ag (I) ions in a molar ratio of 1:1.[39,42]

3.6 | Electrical Conductivity Measurements

All prepared complexes are non-electrolytes due to the absence of any counter ions in their structures. The values of molar conductance are 20.80, 4.00 and 7.70 Ω^{-1} cm^2 mol^{-1} for CuL_2, PdL and AgL, respectively, in DMF at room temperature (Table 4).[30–35]

3.7 | Magnetic Measurements

The geometric structure of the prepared complexes was confirmed using magnetic measurements. The observed magnetic moments for the prepared complexes are listed in Table 4. The CuL_2 complex is paramagnetic and has an octahedral geometry corresponding to one electron pair.[44] The PdL and AgL complexes are diamagnetic and have tetrahedral and square planar geometries, respectively.[42]

3.8 | Mass Spectra

Mass spectra were obtained at 250°C and 70 eV in electron ionization mode. The observed molecular ions peaks are in good agreement with results from elemental analyses (Figure 3, and Figures S7 and S8). The mass spectra of complexes confirm their stoichiometry.[39]

3.9 | Thermogravimetric Analysis

Thermal analysis was used to evaluate the stability of the metal complexes and the existence of water molecules inside or outside the central metal ion coordination sphere.[30] The thermograms of the studied complexes indicate the presence of one hydrated and two coordinated water molecules in the CuL_2 complex, one molecule of coordinated water in the PdL complex and two

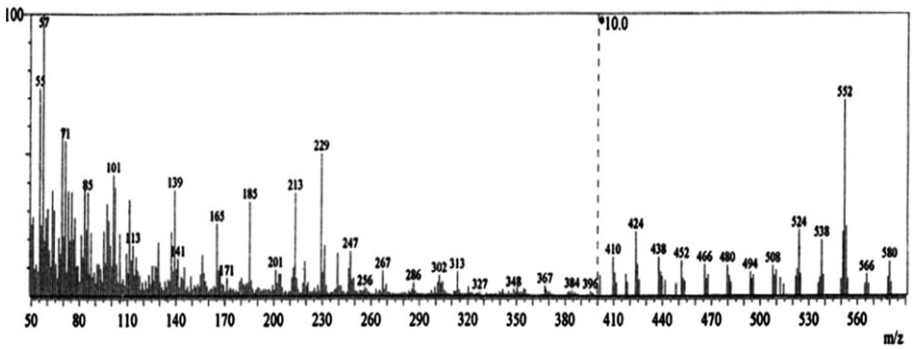

FIGURE 3 Mass spectrum of the CuL_2 complex

molecules of coordinated water in the AgL complex. The thermal behaviour of the studied complexes shows loss of hydrated or/and coordinated water molecules in the first step; then degradation of the HL molecule in the next step (Table 5).

The thermogram of CuL_2 shows five degradation steps within the range 37–608°C. The first stage at 37–196°C corresponds to the elimination of one hydrated and two coordinated water molecules with mass loss of 9.25% (calcd 9.32%). The second stage at 200–300°C corresponds to the removal of part of the ligand (C_6H_4Cl) with mass loss of 19.35% (calcd 19.28%). The third stage at 300–433°C corresponds to the removal of part of HL (C_7H_5NCl) with mass loss of 23.85% (calcd 23.94%).The fourth stage at 435–540°C corresponds to the removal of part of HL (C_6H_4O) with mass loss of 15.99% (calcd 15.91%). The fifth stage at 540–608°C corresponds to the removal of other parts of the ligand with mass loss of 17.72% (calcd 17.81%) to give CuO as a residue.

The thermal analysis curve of the PdL complex shows four degradation steps within the range 37–614°C. The first stage at 37–160°C corresponds to the elimination of one coordinated water molecule with mass loss of 4.47% (calcd 4.35%). The second stage at 165–280°C corresponds to the removal of (CH_3COO^-) group with mass loss of 14.36% (calcd 14.25%). The third stage at 285–440°C corresponds to the removal of part of the ligand (C_7H_5NCl) with mass loss of 33.38% (calcd 33.47%). The fourth step at 444–614°C includes the loss of the other parts of the ligand to finally give PdO as a residue.

The thermal behaviour of the AgL complex shows three degradation steps in the range 37–630°C. The first stage at 37–218°C corresponds to the elimination of two coordinated water molecules with mass loss of 9.69% (calcd 9.60%). The second stage at 220–420°C corresponds to the removal of part of the ligand (C_7H_5Cl) with mass loss of 33.20% (calcd 33.30%). The third step within the range 420–630°C involves removal of organic ligand moiety to finally give ½Ag_2O as a residue with a net weight loss of 30.79% (calcd 30.90%).

3.9.1 | Kinetic parameters for thermal degradation of complexes

The energy of activation ($E^{\neq}$), Arrhenius constant (A), entropy of activation ($\Delta S^{\neq}$), enthalpy of activation ($H^{\neq}$) and free energy change ($\Delta G^{\neq}$) were determined by the Coats–Redfern relation. The obtained data are given in Table 5. In most thermal steps, $S^{\neq}$ values are negative suggesting degradation through an abnormal pathway for those steps and the degradation processes are unfavourable. The $H^{\neq}$ values are positive indicating that degradation processes are endothermic.[30–33,37] It is evident that the $G^{\neq}$values increase with increasing temperature. The negative values of activation entropy show a great activated state. This can occur through oxygen chemisorption and other decomposition products. The activated state can be indicated by the polarization bonds which occur through electronic transitions.

3.10 | Stability Range of Complexes

The pH profile (absorbance versus pH) shows typical dissociation curves and a high stability range of pH (5–10) for the synthesized complexes (Figure 4). The results indicate that the synthesized complexes are more stable

TABLE 5 Thermogravimetric analysis and parameters of thermokinetic activation of each decomposition step for the complexes

Complex	Dec. temp. (°C)	Weight loss (%) Calcd	Found	Dec. assignment	$E^{\neq}$ (kJ mol^{-1})	A (× 10^4 s^{-1})	$\Delta S^{\neq}$ (J mol^{-1})	$\Delta H^{\neq}$ (k J mol^{-1})	$\Delta G^{\neq}$ (kJ mol^{-1} K^{-1})
CuL_2	35–196	9.32	9.25	$3H_2O$	12	7.2	−17.86	10.37	13.87
	200–300	19.28	19.35	C_6H_4Cl			−18.28	9.50	14.98
	300–433	23.94	23.85	C_7H_5NCl			−18.65	8.40	16.47
	435–540	15.91	15.99	C_6H_4O			−18.87	7.51	17.94
	540–608	17.81	17.72	C_7H_5N			−18.99	6.94	18.48
Residue	>608	13.74	13.84	CuO			—	—	—
PdL	37–160	4.35	4.47	H_2O	18	2.7	−18.63	16.67	19.65
	165–280	14.25	14.36	CH_3COO^-			−19.19	15.67	21.04
	285–440	33.47	33.38	C_7H_5NCl			−19.64	14.34	22.98
	444–614	18.37	18.29	C_6H_4			−19.98	12.89	25.16
Residue	<614	29.56	29.50	PdO			—	—	—
AgL	37–218	9.60	9.69	$2H_2O$	25	3.0	−18.84	23.23	27.34
	220–420	33.20	33.10	C_7H_5Cl			−19.49	21.51	29.70
	420–630	24.30	24.40	C_6H_4NO			−19.90	19.76	32.30
Residue	<630	30.90	30.79	½Ag_2O			—	—	—

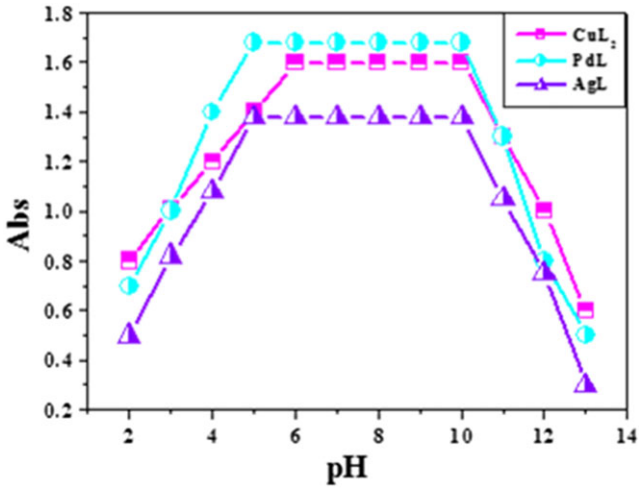

FIGURE 4 pH profiles of the metal complexes in DMF

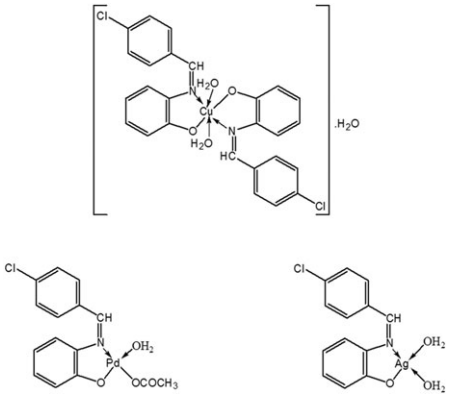

SCHEME 1 Suggested structures of new metal complexes

compared to the ligand.[41,43,44] Consequently, the desired pH range for various applications of the synthesized complexes is pH = 5–10.

Based on the obtained results of elemental analyses, IR and electronic spectra, and molar conductance and magnetic measurements, the suggested structures for the synthesized complexes were identified (Scheme 1).

3.11 | Molecular Orbital Calculations

The optimized geometrical parameters, natural charges on active centres, natural configuration of the metal ions and energetics of the ground state for the studied 1:1 and 1:2 complexes were calculated and discussed using B3LYP/GENECP. From the elemental analysis and spectroscopic data, metal ions are coordinated to the ligand via N7 and O12 atoms, two water molecules in the case of AgL and one water and one acetate anion in the case of PdL, forming diamagnetic 1:1 square planar and tetrahedral complexes, respectively. In the case of the 1:2 copper complex, the metal ion coordinated to the ligand via N7, O16, N21 and O18 atoms and two water molecules forming a paramagnetic distorted octahedral complex.

3.11.1 | Geometry of ligand

The ligand studied in this work and its anion were optimized using the B3LYP/6-311G** level of theory. Energy gap (E_g), and natural charge on active centres are presented in Figure 5. For the computed energy gap, as the energy gap decreases, the reactivity of the compound increases. In our case, E_g of the anion is less than that of the neutral ligand by 2.65 eV (*ca* 61 kcal mol^{-1}), i.e. the anionic form of the ligand is more chemically reactive than the neutral form in the reaction medium and hence interacts with the metal ion to form the studied complexes. The natural charges computed from the NBO analysis show that the most negative centres for chelation in the ligand and its anion are N7 and O9 atoms. In the case of the anion, the natural charge on N7 and O9 atoms increased by 0.028*e* and 0.03*e*, respectively.

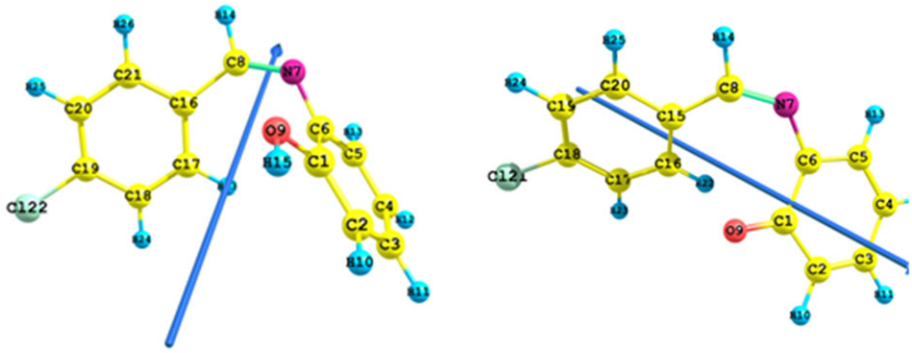

FIGURE 5 Optimized structure, vector of the dipole moment, numbering system, energy gap and natural charge on active centres of the ligand and its anion using B3LYP/6-311G**

These results confirm that these two centres coordinated with the central positive metal ion to form 1:1 and 1:2 complexes.

3.11.2 | Geometry of complexes

The optimized geometry, numbering system, vector of the dipole moment, bond lengths, bond angles and dihedral angles of all 1:1 and 1:2 metal complexes studied in this work are presented in Table S1 and Figure 6. In the AgL complex, the metal ion coordinates with O12 and N7 atoms of the ligand to form a five-member ring, namely AgN7C6C5O12, and with two water molecules, via O27 and O28 atoms, to form a diamagnetic square planar structure (Figure 6). In the case of the PdL complex, the metal ion coordinates with N7 and O12 atoms to form a five-member ring, namely PdN7C6C5O12, and with one water molecule via O26 atom and one acetate group O29 to form a diamagnetic tetrahedral structure. On the other hand, the CuL_2 complex coordinates with N7 and O16 atoms to form a five-member ring, namely CuN7C1C2O16, with N21 and O18 atoms to form a five-member ring, CuO18C19C20N21, and with two water molecules via O48 and O49 atoms to form a paramagnetic distorted octahedral structure. There is a good agreement between the experimental X-ray bond lengths[49–51] obtained for some related complexes (Ag—N, Cu—N and Pd—N are 2.230, 1.960 and 1.730 Å, respectively, and Ag—O, Cu—O and Pd—O are 2.320, 1.956 and 1.904 Å, respectively) and the computed bond lengths at the B3LYP/6-311G** level of theory (Table S1). In our studied complexes, most of the M—N and M—O bonds show elongation upon complexation. The elongation of the M—O bond is greater in AgL and the M—N bonds in 1:2 Cu complex. The length of the coordinate covalent bonds between metal and ligand site, i.e. M—N and M—O, is too long compared to the typical MX (X = O or N) bond length.[52]

The too long M—O and M—N bonds in the complexes mean that the ionic character of these bonds is small. The bond angles computed theoretically at the B3LYP/6-311G** level in our studied complexes are listed in Table S1. The bond angles in CuL_2 vary between 84° and 97° which compare nicely with the experimental data

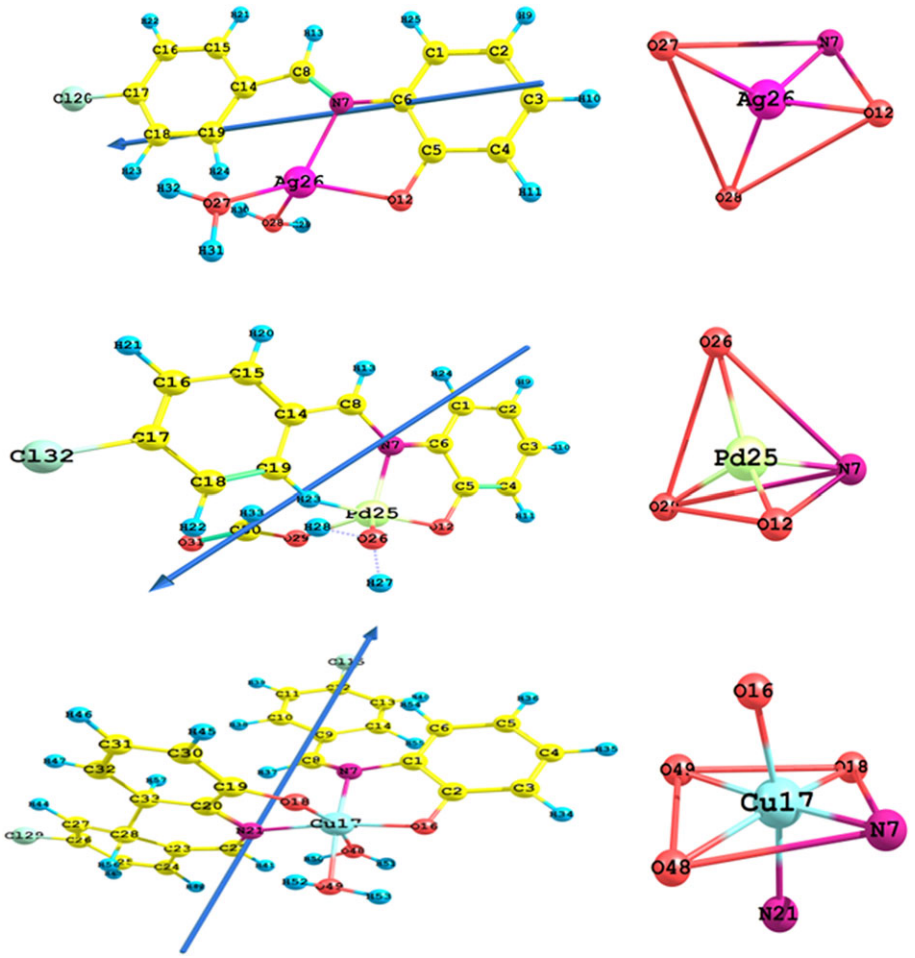

FIGURE 6 Optimized structure, vector of the dipole moment and numbering system for the complexes using B3LYP/GENECP

as obtained from X-ray analysis for O_h complexes.[53] The obtained values of the bond angles show a distorted octahedral geometry. Whereas, the bond angles in AgL vary between 108° and 124° and in the case of PdL between 107° and 119°. The values of the dihedral angles around metal ion in the coordination sphere in the studied complexes (Table S1) are far from 0° or 180° which indicate that the metal ion is not in the same plane as the donating sites, i.e. the studied complexes are non-planar.

3.11.3 | Natural charges and natural population

The natural charge on the coordinated centres before and after complexation and the natural population of the electrons of each metal ion in the core, valence and Rydberg sub-shells and natural electronic configuration of the metal ions in the coordination sphere of 1:1 and 1:2 complexes are presented in Tables 6 and 7. The most electronegative charges are accumulated on O12 and N7 atoms of the ligand in the 1:1 complexes and on O16, O18, N7 and N21 atoms in the 1:2 complex. These electronegative atoms in the coordination sphere have a tendency to donate electrons to the central metal ions. It is observed from the data in Tables 6 and 7 that the negative charges of the coordinated atoms increase after complexation. This may be referred to the back-donation of the charge from the metal ion to the coordinated atoms of the ligand of CuL_2 and AgL. The amounts of the increases in the natural charge on each atom of the coordination sphere and the metal-to-ligand back-donation are listed in Table 6. The total amount of the charges transferred from Ag to L is 0.175*e* and from Cu to L is 0.262*e*. Whereas, the most electropositive atoms, Ag, Pd and Cu, have a tendency to accept electrons from the coordinated atoms of the ligand. In the 1:1 PdL and AgL complexes, the Ag ion received 0.3594*e* ($3d^{9.91}$) and Pd ion received 0.3568*e* ($3d^{8.75}$). Whereas, for 1:2 CuL_2 complex, the Cu ion received 1.0628*e* ($3d^{9.29}$) from the active sites of the ligands (Table 7).

TABLE 6 Natural charge on coordinated centres of the complexes

Centre	HL	CuL_2	PdL	AgL
O12	−0.703		−0.541	−0.787
M → L				0.084
N7	−0.447		−0.396	−0.539
M → L				0.092
O27				−0.961
O28				−0.968
O16	−0.703	−0.719		
M → L		0.016		
N7	−0.447	−0.520		
M → L		0.073		
N21	−0.447	−0.564		
M → L		0.117		
O18	−0.703	−0.759		
M → L		0.056		
O48		−0.940		
O49		−0.958		
O26			−0.935	
O29			−0.676	

3.11.4 | Global reactivity descriptors

The frontier molecular orbital energies of the studied 1:1 and 1:2 complexes were calculated using B3LYP/GENECP and are presented in Table S2 and Figure 7. E_{HOMO} of the studied complexes which measures the donating property follows the order Ag > Cu > Pd. The accepting property of the studied complexes which is represented by E_{LUMO} follows the order Ag >Cu >Pd. The energy gap (E_g) between HOMO and LUMO of the studied complexes characterizes the molecular chemical stability (reactivity). The results in Figure 7 and Table S2 indicate that the smaller the energy gap of the complexes, the easier the charge transfer and the polarization within the molecule. The order of decreasing reactivity in the studied complexes is PdL >>CuL_2 >AgL. Using HOMO and LUMO energies, ionization potential and electron affinity can be expressed as $I \sim -E_{HOMO}$ and $A \sim -E_{LUMO}$ (Table S2). The variation of electronegativity

TABLE 7 Natural charge, natural population and natural electronic configuration of the metal ions for the complexes

Complex	Natural charge	Natural population				Natural electronic configuration
		Core	Valence	Rydberg	Total	
CuL_2	0.9372	17.99	10.057	0.0124	28.063	Core $4s^{0.26}3d^{9.29}4p^{0.51}5p^{0.01}$
PdL	0.6432	35.97	9.364	0.0128	45.356	Core $5s^{0.21}4d^{8.75}5d^{0.01}6p^{0.41}$
AgL	0.6405	35.99	10.356	0.0089	46.359	Core $5s^{0.21}4d^{9.91}5p^{0.01}6p^{0.24}$

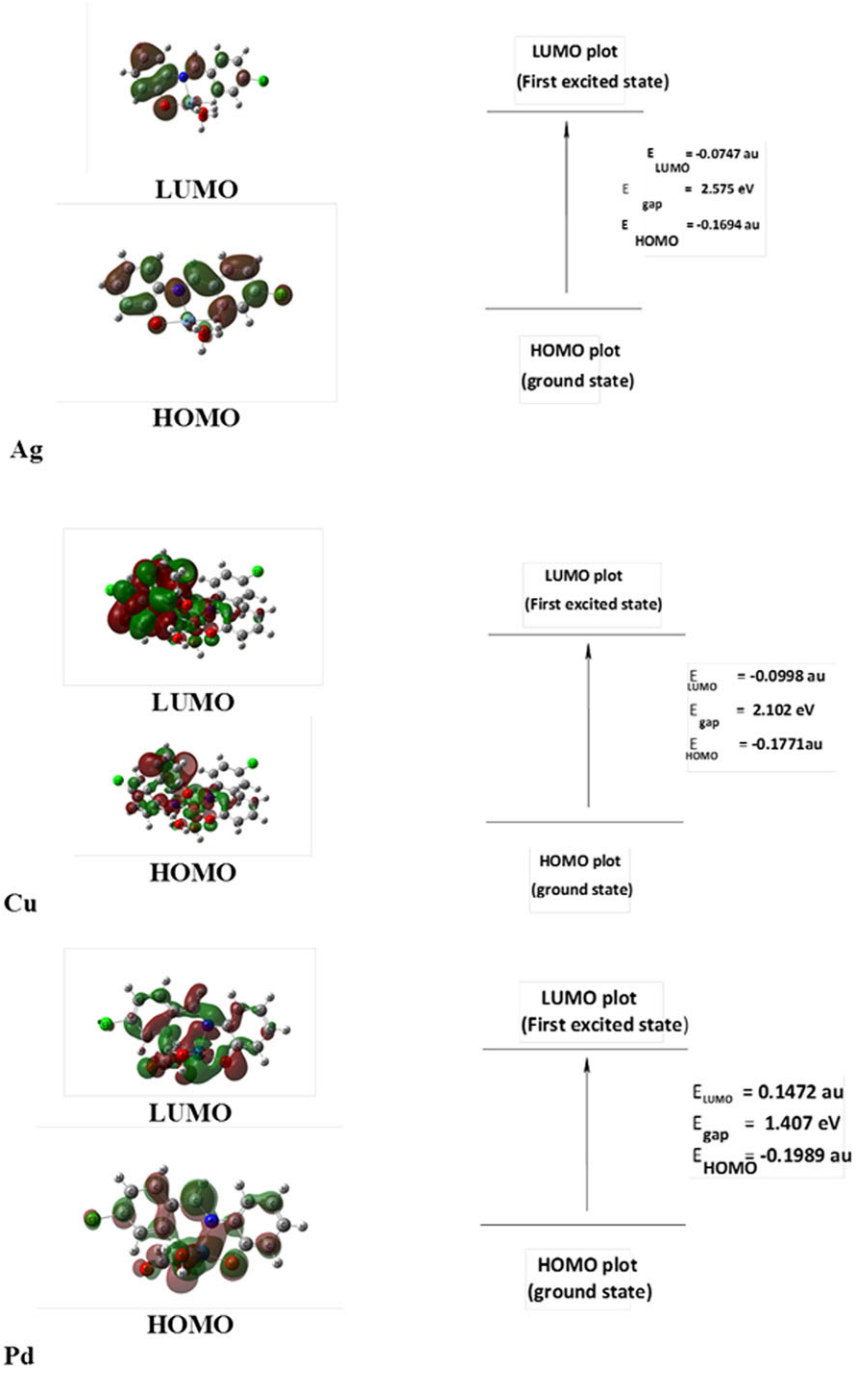

FIGURE 7 HOMO and LUMO charge density maps of the complexes using B3LYP/GENEC

(χ) values is supported by electrostatic potential, the results in Table S2 showing that the order of decreasing χ (increasing charge transfer within the studied complexes) is CuL_2 > AgL >> PdL. The chemical hardness (η) = $(I - A)/2$, electronegativity (χ) = $(I + A)/2$, chemical potential (V) = $-(I + E)/2$ and chemical softness (S) = $1/2\eta$ were calculated and are presented in Table S2. The small η values for the studied complexes reflect the ability of charge transfer inside the studied complexes. The order of decreasing charge transfer within the studied complexes is CuL_2 > AgL >>PdL. The order of decreasing chemical softness S in the studied complexes is CuL_2 >AgL >>PdL.

3.11.5 | NLO properties

No experimental or theoretical investigations were found addressing NLO properties for the ligand and the studied complexes; therefore, this triggered our interest to undertake this study. In order to study the relationship between molecular structure and NLO properties, the polarizabilities α, $\Delta\alpha$ and hyperpolarizabilities (β) of the ligand

and the studied complexes were calculated using B3LYP/GENECP and the results are listed in Table 8. The polarizabilities and first-order hyperpolarizabilities are reported in atomic units (au), the calculated values have been converted into electrostatic units (esu) using a conversion factor of 0.1482×10^{-24} esu for $\alpha$and 8.6393×10^{-33} esu for β. *p*-Nitroaniline (PNA) is a standard prototype used in NLO studies.[54,55] In this study, PNA was chosen as a reference as there were no experimental values of NLO properties of the studied ligand and complexes. The magnitude of $\beta$is one of the key factors in an NLO system. The analysis of βcomputed theoretically for the ligand and the studied complexes indicated that the value for the ligand is 92 times greater than that of the reference PNA indicating that the HL has promising NLO properties. The value of $\beta$for the ligand increases upon complexation. The value for the AgL complex is 440 times greater than that for PNA, and the value for the CuL_2 complex is 7653 times greater and for the PdL complex is 774 times greater than that for PNA (Table 8). Therefore, the studied complexes are promising candidates for NLO materials.

3.12 | Antimicrobial Bioassay for Complexes

The ligand and its complexes were examined against three strains of bacteria and against three strains of fungi.[31,32] The results are reported in Tables 9 and 10 and shown in Figures 8, 9, S9 and S10. All examined compounds show good antimicrobial activity against the microorganisms. It is observed that the complexes

TABLE 8 Total static dipole moment (μ), mean polarizability (α),anisotropy of polarizability ($\Delta\alpha$) and first-order hyperpolarizability (β) for the studied complexes

Property	PNA	HL	CuL_2	PdL	AgL
μ_x		−4.351	−3.855	0.920	6.934
μ_y		0.652	1.554	6.604	−0.246
μ_z		−2.088	−4.716	4.835	0.808
μ_{1D}	2.44	4.871	6.286	8.238	6.968
α_{xx}		−147.3	−219.9	−138.3	−149.7
α_{xy}		−5.6	3.08	−1.29	−11.13
α_{yy}		−107.8	−235.2	−132.4	15.19
α_{zz}		−111.2	12.6	−12.1	6.59
α_{xz}		−3.7	−0.64	−9.3	−1.28
α_{yz}		3.5	13.9	−20.1	4.08
$(\alpha)_1$au		−122.1	−153.5	−94.266	−42.64
$(\alpha)_1$esu	22×10^{-24}	1.809×10^{-23}	2.274×10^{-23}	-1.397×10^{-23}	-6.319×10^{-24}
$\Delta\alpha$au		37.914	240.515	123.355	160.762
$\Delta\alpha$esu		5.6189×10^{-24}	3.5644×10^{-23}	1.828×10^{-23}	2.3825×10^{-23}
β_{xxx}		−34.5	100.5	135.01	−53.58
β_{xxy}		23.6	−93.4	24.8	−23.43
β_{xyy}		−23.7	−41.7	3.4	41.37
β_{yyy}		−10.6	−171.6	−8.2	−97.26
β_{xxz}		8.8	42.6	16.6	−3.29
β_{xyz}		−4.02	4.12	19.6	6.27
β_{yyz}		4.3	−20.8	−25.1	−30.27
β_{xzz}		−13.9	−42.9	5.6	23.58
β_{yzz}		2.3	−33.5	37.8	−75.07
β_{zzz}		−1.3	−67.8	33.9	29.52
β au		165.5182	13731	1389.24	790.952
β esu	15.5×10^{-30}	1.4299×10^{-27}	1.1862×10^{-25}	1.2×10^{-26}	6.8330×10^{-27}

TABLE 9 Results of antibacterial bioassay of HL and its metal complexes

Compound	Inhibition zone (mm)					
	E. coli (−ve)		*B. subtilis* (+ve)		*S. aureus* (+ve)	
Conc. (mg ml^{-1})	10	20	10	20	10	20
HL	4 ± 0.23	8 ± 0.05	5 ± 0.17	13 ± 0.27	4 ± 0.63	11 ± 0.88
CuL_2	14 ± 0.53	29 ± 0.66	17 ± 0.09	39 ± 0.13	15 ± 0.07	35 ± 0.39
PdL	13 ± 0.22	28 ± 0.76	16 ± 0.91	36 ± 0.32	14 ± 0.61	33 ± 0.08
AgL	17 ± 0.29	33 ± 0.11	20 ± 0.19	45 ± 0.87	13 ± 0.33	38 ± 0.41
Gentamycin	20 ± 0.71	40 ± 0.33	26 ± 0.15	51 ± 0.72	25 ± 0.93	45 ± 0.11

TABLE 10 Results of antifungal bioassay of HL and its metal complexes

Compound	Inhibition zone (mm)					
	T. rubrum		*A. flavus*		*C. albicans*	
Conc. (mg ml^{-1})	10	20	10	20	10	20
HL	5 ± 0.05	8 ± 0.55	4 ± 0.11	7 ± 0.82	3 ± 0.10	5 ± 0.04
CuL_2	16 ± 0.22	28 ± 0.10	15 ± 0.22	25 ± 0.14	11 ± 0.10	21 ± 0.19
PdL	14 ± 0.33	25 ± 0.14	12 ± 0.55	23 ± 0.9	9 ± 0.10	18 ± 0.59
AgL	19 ± 0.25	32 ± 0.41	17 ± 0.29	29 ± 0.19	14 ± 0.12	23 ± 0.80
Fluconazole	24 ± 0.55	37 ± 0.62	16 ± 0.49	31 ± 0.88	15 ± 0.71	25 ± 0.90

are more active than the free ligand and this activity is promoted on coordination with metal ions.[56,57] However, the complexes have moderate activity as compared with standards drugs. This promotion in the activity may be dependent on the basis that the ligand has a carbon–nitrogen double bond. The activity of the complexes is greater than that of the ligand and can be explained in terms of chelation theory.[58,59] It is observed that in the complexes, the metal has a positive charge, so it is moderately mutual with the donor atoms present in the Schiff base ligand and there may be π-electron delocalization over the whole chelate. This chelation gives rise to a lipophilic property for the metal complexes and assists their permeation through the

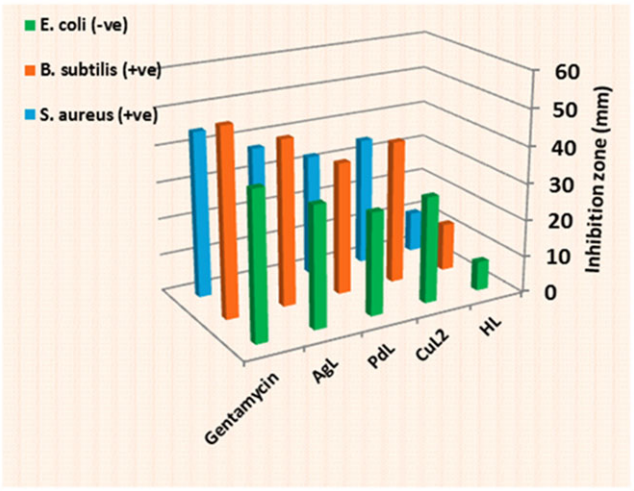

FIGURE 8 Histogram showing the comparative antibacterial activities of HL and its complexes at a concentration of 20 mg ml^{-1}

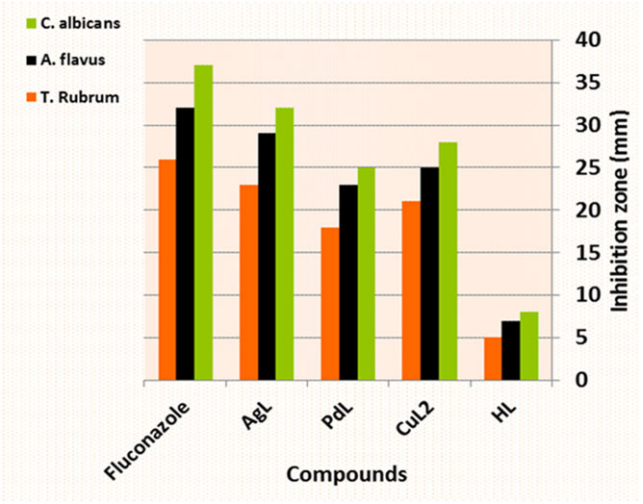

FIGURE 9 Histogram showing the comparative antifungal activities of HL and its complexes at a concentration of 20 mg ml^{-1}

TABLE 11 MIC of HL and its complexes against bacterial and fungal strains

Compound	MIC of bacteria and fungi (mg ml^{-1})					
	E. coli (−ve)	*B. subtilis* (+ve)	6.25	*C. albicans*	*A. flavus*	*T. rubrum*
HL	7.75	6.50	3.00	6.00	6.25	7.50
CuL_2	3.50	2.75	3.25	2.50	2.75	3.25
PdL	3.50	3.00	2.00	2.75	3.00	3.25
AgL	2.50	1.50	6.25	1.25	1.75	2.25

TABLE 12 Activity index of HL and its complexes against bacterial and fungal strains

Compound	Activity index (%)					
	S. aureus (+ve)	*B. subtilis* (+ve)	*E. coli* (−ve)	*C. albicans*	*A. flavus*	*T. rubrum*
HL	20.00	25.49	24.44	21.62	21.87	19.23
CuL_2	72.50	76.47	77.77	75.67	78.12	80.70
PdL	70.00	70.58	73.33	67.56	71.87	69.23
AgL	82.50	88.23	84.44	86.48	90.62	88.46

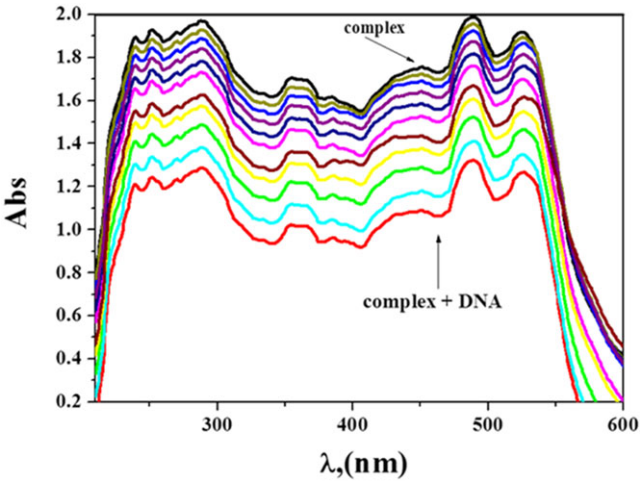

FIGURE 10 Electronic absorption scans for binding of DNA with PdL complex (10^{-3} M) in 0.01 M Tris buffer (pH = 7.2, 298 K) with CT-DNA (0–100 μM, from bottom to top)

lipid layer of the membranes of bacteria. Also, other factors should be considered such as solubility, activity, conductivity and bond length between the metal and ligand. Minimum inhibitory concentration (MIC) profiles of the studied compounds against selected strains of bacteria and fungi are summarized in Table 11. The MIC values of HL and its complexes against the selected strains of bacterial and fungi indicated that HL has lower antimicrobial activity than its complexes. The activities for the compounds were confirmed by calculating the potency index (Table 12) according to the following relation[30–35]:

$$\text{Activity index}\ (\%) = \frac{\text{Inhibition zone of compound (mm)}}{\text{Inhibition zone of standard (mm)}} \times 100 \quad (20)$$

3.13 | Binding of Complexes with CT-DNA

3.13.1 | Electronic spectroscopy for interaction of complexes with CT-DNA

Electronic absorption spectroscopy is an important method for studying DNA binding with metal complexes. DNA binding is in three types: (i) binding interaction between two grooves of the DNA double helix; (ii) intercalation between the stacked base pairs of native DNA; and (iii) electrostatic interaction with the negatively charged nucleic sugar–phosphate structure, which is along the external DNA double helix and does not have selectivity.[32–35,38,39,60] The absorption spectral data for the interaction DNA with the complexes through intercalation shows significant hypochromicity and a red-shift due to the strong $\pi \rightarrow \pi^*$ transition due to interaction between the base pairs of DNA and the aromatic chromophore ligand of metal complexes (Figure 10, and Figures S11 and S12).[61] The spectra were obtained as a function of the addition of buffer solutions of pure CT-DNA to buffer solutions of the studied complexes. The π–π^* transition energy is lowered when the orbital of the inserted ligand couples with the orbital of the base pairs and this leads bathochromicity, so the interaction is via intercalation

TABLE 13 Spectroscopic parameters and K_b results for DNA interaction with the complexes

Complex	λ_{max} free (nm)	λ_{max} bound (nm)	Δn	Chromism (%)[a]	Type of chromism	Binding constant ($\times 10^5$)	ΔG (kJ mol^{-1})
CuL_2	239	242	3	5.29			
	252	255	2	5.69	Hypo		
	361	364	3	5.88		3.10	−31.33
	483	486	3	5.29			
PdL	239	242	3	2.12			
	252	254	2	2.08	Hypo		
	489	492	3	1.52		1.27	−29.12
	525	527	2	1.05			
AgL	239	242	3	2.00			
	501	503	2	11.76	Hypo	1.16	−28.89

[a]Chromism (%) = $(Abs_{free} - Abs_{bound})/Abs_{free}$.[30–35]

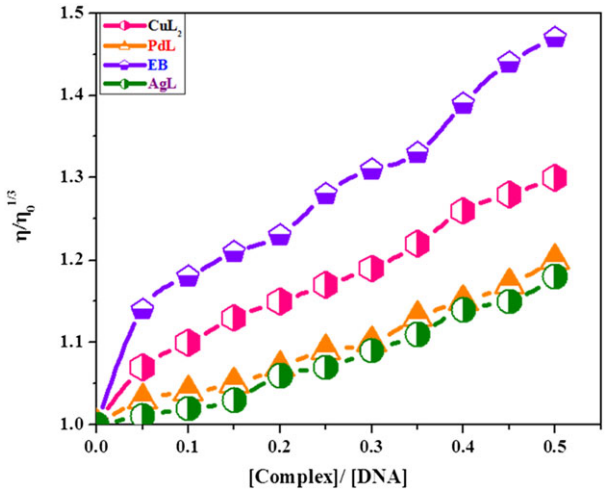

FIGURE 11 Dynamic viscosity measurements of the complexes at [DNA] = 0.5 mM ([complex] and [ethidium bromide] = 25–250 μM at 298 K)

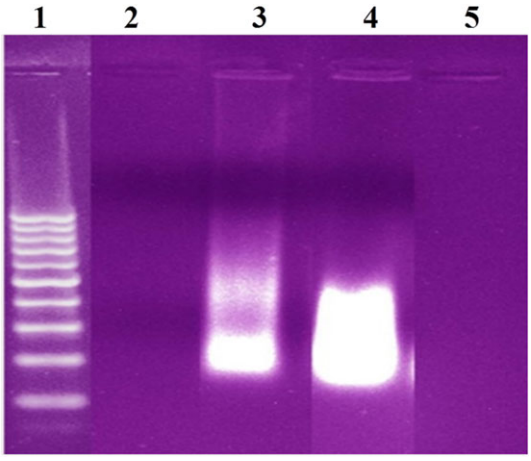

FIGURE 12 Gel electrophoresis results for DNA in the presence of the metal complexes. Lane 1: DNA ladder; lane 2: PdL complex + CT-DNA; lane 3: AgL complex + CT-DNA; lane 4: CuL_2 complex + CT-DNA; lane 5: PdL complex

mode. When the conjugation orbital is partially filled by electrons, this leads to a reduction in the transition probabilities and so leading to hypochromicity. The spectroscopic parameters and K_b for the DNA interaction with the synthesized complexes are listed in Table 13. K_b was calculated from the ratio of slope to intercept (Figures S13–S15). The synthesized metal complexes could bind to DNA mainly through the intercalative mode through the series CuL_2 >PdL >AgL.

3.13.2 | Viscosity measurements for interaction of complexes with CT-DNA

Dynamic viscosity measurements are used to study the binding mode of metal complexes with DNA.[30–35,37,60] Under suitable conditions, the intercalation of compounds such as ethidium bromide leads to a significant increase in the DNA viscosity because of an increase in the isolation of base pairs at the intercalation sites and hence an increase in the overall DNA length.[62] With an increasing amount of complexes, the relative viscosity of CT-DNA increases indicating that these complexes can bond with CT-DNA via intercalation mode as shown in Figure 11.[42] These viscosity measurements show that all the synthesized complexes can intercalate among adjacent CT-DNA base pairs causing an extension in the DNA helix and thus increasing the viscosity with increasing complex concentration.

TABLE 14 Details of docked Schiff base metal complexes

Code	k_b	S	E_{conf}
CuL_2	3.10	−6.0040	−955.3530
PdL	1.27	−5.2442	−191.6363
AgL	1.16	−4.8835	−101.1103

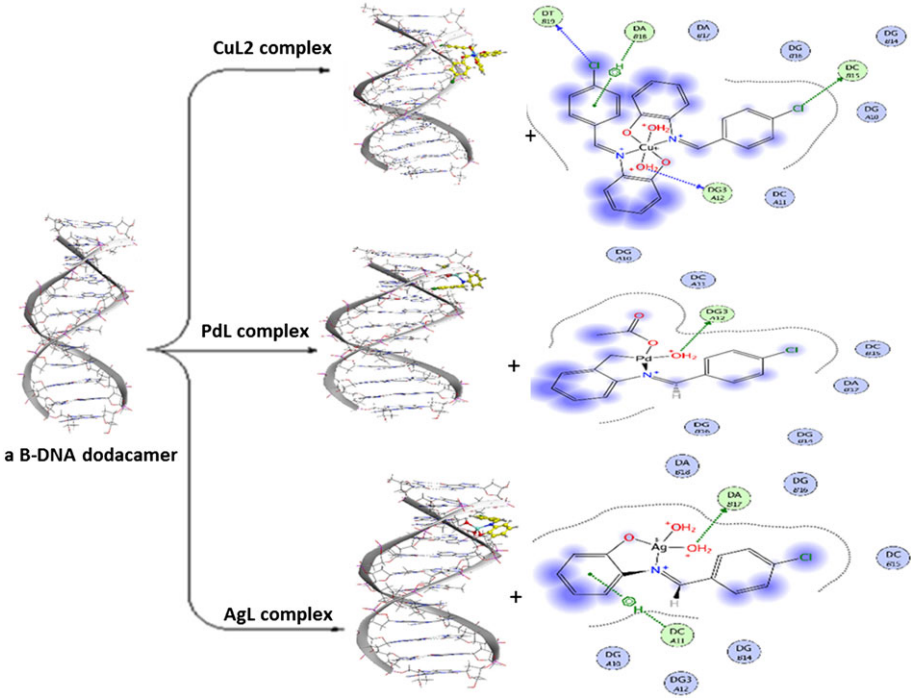

FIGURE 13 Three-dimensional plots and corresponding two-dimensional plots of interaction of the complexes with DNA

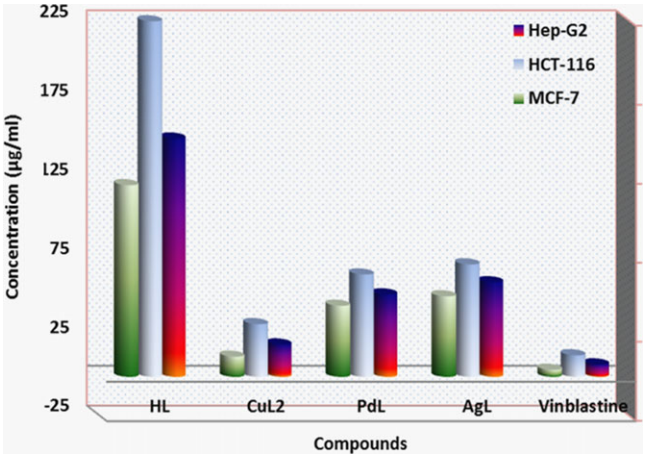

FIGURE 14 IC_{50} values for HL, its metal complexes and vinblastine drug against Hep-G2, MCF-7 and HCT-116 cell lines

3.13.3 | Gel electrophoresis for interaction of complexes with CT-DNA

Gel electrophoresis is a method used to study the interaction DNA with complexes.[31–35,60] The gel after electrophoresis showed that the intensity of the DNA treated with the complexes has partially decreased in CuL_2 and AgL, and, in contrast, disappears in PdL, possibly because of the complete cleavage of DNA[63] (Figure 12). From DNA binding with the investigated complexes, it can be derived that the studied complexes lower the growth of a pathogenic organism by interaction with the genome.

3.14 | Molecular Docking

Molecular docking is a great approach for understanding the interaction between investigated complexes and a biological target which is important in medical treatment. In our investigation, the synthesized complexes were studied by molecular docking using MOE version 2016.08 to understand the drug–DNA interactions to explore the potential binding mode and energy. Docked ligand conformation was evaluated according to hydrogen bonding, binding energy and hydrophobic interaction between the synthesized complexes and B-DNA (PDB ID: 1BNA). From the docking scores, the details of the docked complexes were obtained (Table 14).

The docking studies showed that the prepared docked complexes fit mainly in the DNA minor groove and involve hydrophobic as well as hydrogen bonding interactions with DNA bases. Most of the optimal results of docking were in the GC region. Binding interactions of the prepared complexes are displayed in Figure 13.

The CuL_2 complex showed the best binding score and energy conformation of −6.0040 and −955.3530 kcal mol^{-1}, respectively, with one π–H interaction and three hydrogen bonds with the DNA. In the CuL_2 complex, the copper metal forms hydrogen-donor bond with

guanine base through one of the complex water molecules while the two *para* chloro groups form hydrogen-donor bonds with cytosine and thymine bases. The distance of the hydrogen bonds was 3.01–4.06 Å.

3.15 | Anticancer Activity of Complexes

The prepared compounds were examined against Hep-G2 cell line (hepatocellular carcinoma), MCF-7 cell line (breast carcinoma) and HCT-116 cell line (colon carcinoma) within the concentration range 0–10 μM. The values for IC_{50} were estimated for HL and its complexes (Figure 14 and Table S3). Cytotoxicity results show that CuL_2, PdL and AgL have an anticancer activity where the IC_{50} values for HCT-116 cell line are in the range 33.4–72.4 μg μl^{-1}, for Hep-G2 cell line are in the range 20.5–59.9 μg μl^{-1} and for MCF-7 cell line are in the range 12.8–51 μg μl^{-1}. It is observed from these results that the prepared complexes are more potent than the ligand and showed manifest anticancer activity compared to vinblastine drug because their biological properties are affected via the complexation locations and the nature of the metal ion which was considered in Tweed's chelation theory.[30–32,64] The positive charge on metal ions increases the acidity of the coordinated ligand and makes stronger hydrogen bonds enhancing the biological activity. The biological activity is also affected by the coordination locations and the nature of the metal modifying the binding ability to DNA.[30–32]

4 | CONCLUSIONS

In this study three new Cu (II), Pd (II) and Ag (I) complexes have been prepared and characterized via physicochemical measurements, density functional theory calculations and spectral analyses. These results indicated that HL behaves as a N,O bidentate ligand and forms complexes with Pd (II) and Ag (I) ions in a 1:1 molar ratio and with Cu (II) ion in a 1:2 molar ratio. The PdL and AgL complexes are diamagnetic and have tetrahedral and square planar geometry, respectively, while the CuL_2 complex is paramagnetic and has a distorted octahedral geometry. All the studied complexes are non-planar as reflected in the dihedral angles. The charges of the coordinated centres increase upon complexation and a back-donation from metal to ligand is observed. The calculated values of first-order hyperpolarizability of the ligand and the studied complexes indicate that they are potential candidates for NLO materials. Anti-pathogenic screening demonstrated that the prepared compounds show good antimicrobial activity against various microorganisms as compared to the control. Moreover, the interaction of CT-DNA with the studied complexes has been effectively estimated using electronic absorption, viscosity measurements and gel electrophoresis. The DNA interaction studies suggest that the interaction of these complexes with CT-DNA occurs via intercalative and groove modes. The docking studies showed that the prepared docked complexes fit mainly in the DNA minor groove and involve hydrophobic as well as hydrogen bonding interactions with DNA bases. Most of the optimal results of docking were in the GC region. Furthermore, the growth inhibition effect of the studied compounds was examined against HCT-116, HepG-2 and MCF-7 cell lines. Among these compounds, the CuL_2 complex significantly decreases cell viability in time- and dose-dependent manners. These biological results from our investigation would be beneficial in investigating DNA interaction when exposed to metal complexes and may lead to an improvement in metal-based therapeutic drugs.

ORCID

Laila H. Abdel-Rahman http://orcid.org/0000-0001-7375-2885
Mohamed Shaker S. Adam http://orcid.org/0000-0001-8826-3558
Ahmed M. Abu-Dief http://orcid.org/0000-0003-3771-9011

REFERENCES

[1] D. P. Singh, K. Kumar, C. Sharma, *Eur. J. Med. Chem.* **2010**, *45*, 1230.

[2] L. H. Abdel-Rahman, A. M. Abu-Dief, S. K. Hamdan, A. A. Seleem, *Int. J. Nano Chem.* **2015**, *2*, 65.

[3] L. H. Abdel-Rahman, A. M. Abu-Dief, M. O. Aboelez, A. A. H. Abdel-Mawgoud, *J. Photochem. Photobiol. B* **2017**, *170*, 271.

[4] L. Wang, Y. Feng, J. Xue, Y. Li, *Int. J. Pharm. Technol. Res.* **2008**, *1*, 22.

[5] A. M. Abu-Dief, I. M. A. Mohamed, *Beni-Suef Univ. J. Basic Appl. Sci.* **2015**, *4*, 119.

[6] Y. Prashanthi, S. Raj, *J. Sci. Res.* **2010**, *2*, 114.

[7] Y. K. Gupta, S. C. Agarwal, S. P. Madnawat, R. Narain, *Res. J. Chem. Sci.* **2012**, *4*, 2.

[8] M. Galanski, *Rec. Pat. Anti-Cancer Drug Discov.* **2006**, *1*, 285.

[9] S. P. Kollur, S. K. Linganna, C. Shivamallu, R. M. N. Kumar, H. D. Revanasiddappa, *Spectrochim. Acta A* **2013**, *107*, 108.

[10] E. Gao, C. Liu, M. Zhu, H. Lin, Q. Wu, *Anticancer Agents Med Chem.* **2009**, *9*, 356.

[11] L. H. Abdel-Rahman, A. M. Abu-Dief, R. M. El-Khatib, S. M. Abdel-Fatah, A. A. Seleem, *Int. J. Nano Chem.* **2016**, *2*, 83.

[12] L. Rigamonti, *La Chimica & L'Industria* **2010**, *3*, 118.

[13] H. M. Abd El-Lateef, A. M. Abu-Dief, M. A. A. Mohamed, *J. Mol. Struct.* **2017**, *1130*, 522.

[14] H. M. Abd El-Lateef, A. M. Abu-Dief, B. E. D. M. El-Gendy, *J. Electroanal. Chem.* **2015**, *758*, 135.

[15] H. M. Abd El-Lateef, A. M. Abu-Dief, L. H. Abdel-Rahman, E. C. Sañudo, N. Aliaga Alcalde, *J. Electroanal. Chem.* **2015**, *743*, 120.

[16] L. H. Abdel-Rahman, A. M. Abu-Dief, M. Basha, A. A. H. Abdel-Mawgoud, *Appl. Organometal. Chem.* **2017**, *31*, 3750.

[17] L. H. Abdel-Rahman, A. M. Abu-Dief, M. Ismael, M. A. A. Mohamed, N. A. Hashem, *J. Mol. Struct.* **2016**, *1103*, 232.

[18] A. S. Munde, A. N. Jagdale, S. M. Jadhav, T. K. Chondhekar, *J. Serb. Chem. Soc.* **2010**, *75*, 349.

[19] M.J. Frisch, G.W. Trucks, H.B. Schlegel, G.E. Scuseria, M.A. Robb, J.R. Cheeseman, G. Scalmani, V. Barone, B. Mennucci, G.A. Petersson, H. Nakatsuji, M. Caricato, X. Li, H.P. Hratchian, A.F. Izmaylov, J. Bloino, G. Zheng, J.L. Sonnenberg, M. Hada, M. Ehara, K. Toyota, R. Fukuda, J. Hasegawa, M. Ishida, T. Nakajima, Y. Honda, O. Kitao, H. Nakai, T. Vreven, J.A. Montgomery Jr, J.E. Peralta, F. Ogliaro, M. Bearpark, J.J. Heyd, E. Brothers, K.N. Kudin, V.N. Staroverov, R. Kobayashi, J. Normand, K. Raghavachari, A. Rendell, J.C. Burant, S.S. Iyengar, J. Tomasi, M. Cossi, N. Rega, J.M. Millam, M. Klene, J.E. Knox, J.B. Cross, V. Bakken, C. Adamo, J. Jaramillo, R. Gomperts, R.E. Stratmann, O. Yazyev, A.J. Austin, R. Cammi, C. Pomelli, J.W. Ochterski, R.L. Martin, K. Morokuma, V.G. Zakrzewski, G.A. Voth, P. Salvador, J.J. Dannenberg, S. Dapprich, A.D. Daniels, O. Farkas, J.B. Foresman, J.V. Ortiz, J. Cioslowski, D.J. Fox, Gaussian 09W, Gaussian Inc., Wallingford, CT, **2009**.

[20] T. Schaefer, T. A. Wildman, S. R. Salman, *J. Am. Chem. Soc.* **1980**, *102*, 107.

[21] T. Schaefer, S. R. Salman, T. A. Wildman, P. D. Clark, *Can. J. Chem.* **1982**, *60*, 342.

[22] A. D. Becke, *J. Chem. Phys.* **1993**, *98*, 648.

[23] P. J. Hay, W. R. Wadt, *J. Chem. Phys.* **1985**, *82*, 84.

[24] A. E. Reed, F. Weinhold, *J. Chem. Phys.* **1983**, *78*, 4066.

[25] R. G. Pearson, *Proc. Natl. Acad. Sci. U. S. A.* **1986**, *83*, 8440.

[26] A. K. Chandra, T. Uchimara, *J. Chem. Phys. A* **2001**, *105*, 3578.

[27] X. Chen, F. Yan, M. Wu, H. B. Tian, S. X. Li, X. Shan, K. Wang, Z. Li, K. Xu, *Chem. Phys. Lett.* **2009**, *472*, 19.

[28] D. Avci, *Spectrochim. Acta A* **2011**, *82*, 37.

[29] D. Avci, A. Başoğlu, Y. Atalay, *Struct. Chem.* **2010**, *21*, 213.

[30] L. H. Abdel-Rahman, A. M. Abu-Dief, H. Moustafa, A. A. H. Abdel-Mawgoud, *Arab. J. Chem.* **2017**. in press, DOI: https://doi.org/10.1016/j.arabjc.2017.07.007

[31] L. H. Abdel-Rahman, A. M. Abu-Dief, A. A. H. Abdel-Mawgoud, *J. King Saud Univ.* **2017**. in press, DOI: https://doi.org/10.1016/j.jksus.2017.05.011

[32] L. H. Abdel-Rahman, N. M. Ismail, M. Ismael, A. M. Abu-Dief, E. A. H. Ahmed, *J. Mol. Struct.* **2017**, *1134*, 851.

[33] L. H. Abdel-Rahman, R. M. El-Khatib, L. A. E. Nassr, A. M. Abu-Dief, M. Ismael, A. A. Seleem, *Spectrochim. Acta A* **2014**, *117*, 366.

[34] L. H. Abdel-Rahman, R. M. El-Khatib, L. A. E. Nassr, A. M. Abu-Dief, *J. Mol. Struct.* **2013**, *1040*, 9.

[35] A. M. Abu-Dief, L. A. E. Nassr, *Iran. J. Chem. Soc.* **2015**, *12*, 943.

[36] L. H. Abdel-Rahman, A. M. Abu-Dief, E. F. Newair, S. K. Hamdan, *J. Photochem. Photobiol. B* **2016**, *160*, 18.

[37] A. M. Abu-Dief, I. F. Nassar, W. H. Elsayed, *Appl. Organometal. Chem.* **2016**, *30*, 917.

[38] T. A. Halgren, *J. Comput. Chem.* **1996**, *17*, 490.

[39] L. H. Abdel-Rahman, A. M. Abu-Dief, M. S. S. Adam, S. K. Hamdan, *Catal. Lett.* **2016**, *146*, 1373.

[40] L. H. Abdel-Rahman, R. M. El-Khatib, L. A. E. Nassr, A. M. Abu-Dief, F. E. D. Lashin, *Spectrochim. Acta A* **2013**, *111*, 266.

[41] S. K. Gupta, C. Anjana, N. Sen, R. J. Butcher, J. P. Jasinski, J. A. Golen, *Polyhedron* **2015**, *89*, 219.

[42] K. Y. El-Baradie, N. A. El-Wakiel, H. A. El-Ghamry, *Appl. Organometal. Chem.* **2015**, *29*, 117.

[43] E. M. M. Ibrahim, L. H. Abdel Rahman, A. M. Abu-Dief, R. M. El-Khatib, S. M. Abdel-Fatah, A. M. Adam, *Appl. Organometal. Chem.* **2018**, *3*, e4171.

[44] L. H. Abdel-Rahman, R. M. El-Khatib, L. A. E. Nassr, A. M. Abu-Dief, *Arab. J. Chem.* **2017**, *10*, S1835.

[45] S. S. Shah, R. G. Parmar, *Pharma Chem.* **2011**, *3*, 318.

[46] L. H. Abdel-Rahman, R. M. El-Khatib, L. A. E. Nassr, A. M. Abu-Dief, *Russ. J. Gen. Chem.* **2014**, *84*, 1830.

[47] L. H. Abdel Rahman, A. M. Abu-Dief, N. A. Hashem, A. A. Seleem, *Int. J. Nano Chem.* **2015**, *1*, 79.

[48] L. H. Abdel-Rahman, A. M. Abu-Dief, H. Moustafa, S. K. Hamdan, *Appl. Organometal. Chem.* **2016**, *31*, 3555.

[49] A. Nimmermark, L. Öhrström, J. Reedijk, *Z. Kristallogr.* **2013**, *228*, 311.

[50] A. Martinger, *J. Braz. Chem. Soc.* **2005**, *16*, 39.

[51] I. Persson, K. B. Nilsson, *Inorg. Chem.* **2006**, *45*, 7428.

[52] L. Armelao, S. Quici, F. Brigelletti, G. Accorsi, G. Bottaroi, M. Cavazzini, E. Tendello, *Coord. Chem. Rev.* **2010**, *254*, 487.

[53] S. S. Zumdahl, *Chemistry*, University Science Books, Sausalito, CA **2000**.

[54] L. T. Cheng, W. Tam, S. H. Stevenson, G. R. Meredith, G. Rikken, S. R. Marder, *J. Phys. Chem.* **1991**, *95*, 10631.

[55] P. Kaatz, E. A. Donley, D. P. Shelton, *J. Phys. Chem.* **1998**, *108*, 849.

[56] L. H. Abdel Rahman, A. M. Abu-Dief, R. M. El-Khatib, S. M. Abdel-Fatah, *Bioorg. Chem.* **2016**, *69*, 140.

[57] S. Karabasannavar, P. Allolli, I. N. Shaikh, B. M. Kalshetty, *Indian J. Pharm. Educ. Res.* **2017**, *51*, 490.

[58] R. Ramesh, S. J. Maheswaran, *J. Inorg. Biochem.* **2003**, *96*, 457.

[59] N. Pravin, N. Raman, *Inorg. Chem. Commun.* **2013**, *36*, 45.

[60] L. H. Abdel-Rahman, A. M. Abu-Dief, N. M. Ismail, M. Ismael, *Inorg. Nano-Met. Chem.* **2017**, *47*, 467.

[61] P. Jayaseelan, E. Akila, M. Usha Rani, R. Rajavel, *J. Saudi Chem. Soc.* **2016**, *20*, 625.

[62] L. H. Abdel-Rahman, A. M. Abu-Dief, R. M. El-Khatib, S. M. Abdel-Fatah, *Int. J. Nano Chem.* **2018**, *1*, 1.

[63] A. J. Pearl, T. F. A. F. Reji, *J. Chem. Pharm. Res.* **2013**, *5*, 115.

[64] L. H. Abdel-Rahman, A. M. Abu-Dief, R. M. El-Khatib, S. M. Abdel-Fatah, *J. Photochem. Photobiol. B* **2016**, *162*, 298.

SUPPORTING INFORMATION

Additional supporting information may be found online in the Supporting Information section at the end of the article.

How to cite this article: Abdel-Rahman LH, Adam MSS, Abu-Dief AM, et al. Synthesis, theoretical investigations, biocidal screening, DNA binding, *in vitro* cytotoxicity and molecular docking of novel Cu (II), Pd (II) and Ag (I) complexes of chlorobenzylidene Schiff base: Promising antibiotic and anticancer agents. *Appl Organometal Chem*. 2018;32:e4527. https://doi.org/10.1002/aoc.4527